ACS Energy LETTERS

Open Access

http://pubs.acs.org/journal/aelccp

Photon Statistics as a Tool to (Dis)Prove Cooperative Energy Transfer Quantum Cutting in Near-Infrared Emitting Materials

Vincent R.M. Benning, Nils van de Mortel, Midas Waakop Reijers, Maurits Mastwijk, Sander J.W. Vonk, Andries Meijerink, and Freddy T. Rabouw*

Cite This: *ACS Energy Lett.* 2025, 10, 4620−4626

Read Online

ACCESS | Metrics & More | Article Recommendations | Supporting Information

ABSTRACT: **Spectral conversion of sunlight can enhance solar cell efficiencies by shifting short-wavelength photons to longer wavelengths, where the photovoltaic response is stronger. This can be realized with near 100% energy efficiency by materials capable of *quantum cutting*. These emit two longer-wavelength photons, following the absorption of one shorter-wavelength photon. Although various quantum-cutting materials have been reported, follow-up research has often disproved initial claims. Here, we demonstrate that photon correlation analysis is a universal strategy to unambiguously identify quantum cutting. We investigate two materials, YPO_4 codoped with Tb^{3+} and Yb^{3+} and yttrium aluminum garnet (YAG) codoped with Ce^{3+} and Yb^{3+}. Both are reported to perform quantum cutting via blue light absorption followed by cooperative energy transfer to near-infrared-emitting Yb^{3+}, but some studies have cast doubts for YAG:Ce^{3+},Yb^{3+}. Our correlation analysis demonstrates bunched emission for YPO_4:Tb^{3+},Yb^{3+}, confirming quantum cutting. In contrast, YAG:Ce^{3+},Yb^{3+} shows Poissonian emission statistics, disproving its quantum-cutting capability, despite previous claims.**

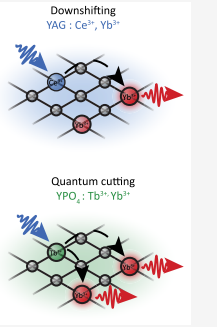

Phosphors are materials that convert light color through absorption and emission. These materials are widely used in displays and lighting technologies to reshape the narrow spectrum of efficient blue LEDs into a broadband spectrum spanning the entire visible range via luminescence downshifting.[1,2] This conversion introduces losses as a result of the energy difference between the differently colored photons. For example, the conversion from a blue photon (450 nm) to a red photon (630 nm) has a theoretical maximum energy efficiency of ∼70%.

Phosphors capable of quantum cutting (QC) are an interesting class that circumvents these energy losses: they absorb high-energy photons and generate multiple lower-energy photons. Quantum cutting allows for color conversion of light with a wavelength of λ into two photons with a wavelength of 2λ, with an energy efficiency that can approach unity.[3−6] A wide variety of mechanisms may give rise to QC, ranging from singlet fission in organic crystals to multiexciton generation in semiconductors (nano)crystals to energy-transfer processes in lanthanide-doped systems.[2−9] Lanthanide-doped inorganic crystals have the benefit that they are stable, nontoxic and have a high overall QC efficiency compared to other QC systems.[10−15]

In the past, lanthanide-based QC materials have been proposed as efficient phosphors for the spectral conversion of vacuum-UV to visible light in plasma displays and fluorescent tubes.[16−19] Nowadays, the scope of QC research has shifted toward the conversion of visible light to near-infrared (NIR), for the use in next-generation photovoltaics. QC phosphors reduce thermalization losses by reshaping the spectrum of solar light ($\lambda \leq 550$ nm) before it enters the solar cell, increasing the short-circuit current output. This spectral conversion can yield an increase of the light-to-electricity conversion efficiency of 8.3 percentage points, surpassing the Shockley−Queisser limit.[20]

The optimal emission wavelength of a QC material for integration with Si photovoltaics is between 900−1100 nm. To this end, Yb^{3+} is a particularly well-suited emitter, as it features a single NIR transition with an emission wavelength of 1000 nm. However, exciting Yb^{3+} with visible light necessitates sensitizaton. Sensitizers with an excited-state energy of twice the Yb^{3+} transition energy have been of considerable interest.[3−6,9] They could, in theory, sensitize two Yb^{3+} ions simultaneously through cooperative energy transfer.

As Yb^{3+} is a 2-level system, it is tempting to interpret any successful sensitization of Yb^{3+} from a UV-, blue- or green-

Received: May 16, 2025
Revised: August 14, 2025
Accepted: August 26, 2025
Published: August 30, 2025

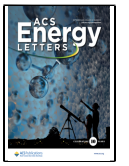

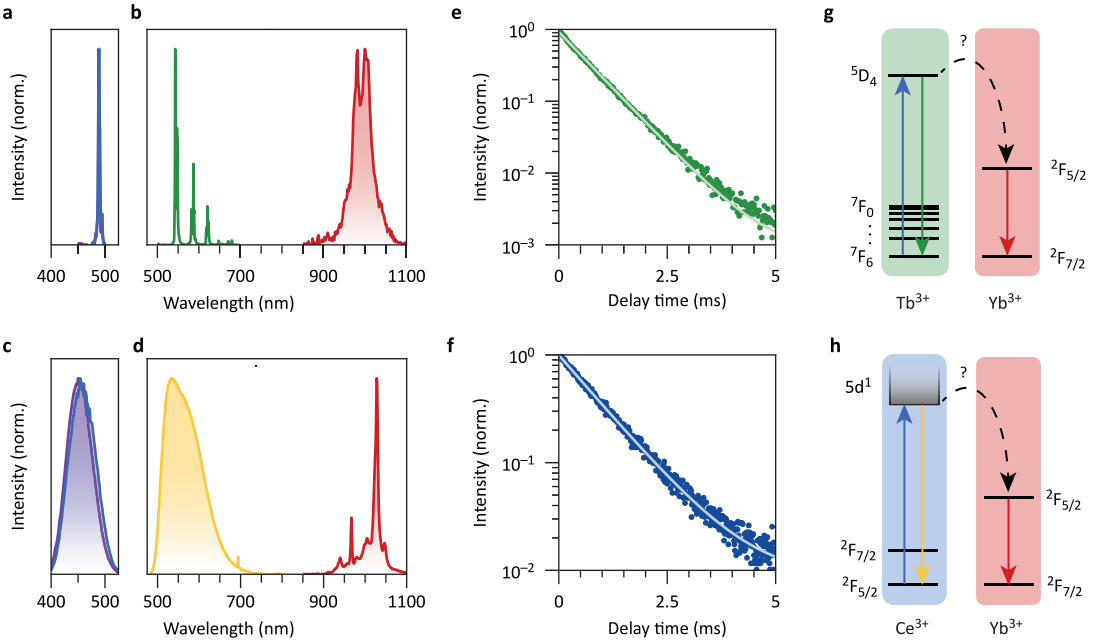

Figure 1. (a–e) Photoluminescence excitation and emission spectra of (a, b) YPO_4:Tb^{3+},Yb^{3+} and (c, d) YAG:Ce^{3+},Yb^{3+}. The excitation plots (panels a and c) show two overlapping spectra, consistent with excitation of the sensitizer and activator by the sensitizer. The sensitizer excitation spectra (purple) are recorded at λ_{em} = 544 nm for YPO_4:Tb^{3+},Yb^{3+} in (a), or at λ_{em} = 570 nm for YAG:Ce^{3+},Yb^{3+} in (c). The Yb^{3+} excitation spectra (blue) are recorded at the maximum emission intensity for the respective host, λ_{em} = 1000 nm for YPO_4 and λ_{em} = 1028 nm for YAG. The emission plots (panels b and d) are recorded upon excitation at λ_{ex} = 488 nm for YPO_4:Tb^{3+},Yb^{3+} in (b), or at λ_{ex} = 445 nm for YAG:Ce^{3+},Yb^{3+} in (d). (e, f) Photoluminescence decay curves (dots) recorded at λ_{em} = 1000–1100 nm and corresponding monoexponential fits (line) of the $Yb^{3+2}F_{5/2} \rightarrow {}^2F_{7/2}$ transition upon resonant excitation with 980 nm light for (e) YPO_4 and (f) YAG. (g, h) Energy-level diagram of Ce^{3+}, Tb^{3+}, and Yb^{3+}. The energy transfer mechanism cannot be inferred based on the emission and excitation spectra or the energy level diagram. However, the sensitizer emission energies lie at 2 times the energy of the $^2F_{7/2} \rightarrow {}^2F_{5/2}$ transition, making cooperative energy transfer energetically possible. The lower QY for the Yb^{3+} emission in YPO_4 can be explained by concentration quenching, which can be expected at a doping concentration of 15%. The lower (5%) doping concentration in YAG does not give rise to concentration quenching.

absorbing sensitizer as QC by cooperative energy transfer. However, multiple studies have found sensitization pathways via an Yb^{2+}-mediated charge transfer state, induced by codopants[21–23] or the semiconductor host.[24,25] These pathways produce just one excited Yb^{3+} per photon absorption event, making these materials downshifting phosphors but not QC phosphors.

Acquiring experimental evidence for cooperative energy transfer in Yb^{3+}-doped materials is not trivial. Still, QC claims are sometimes made based solely on the energy level scheme of the sensitizer and the observation of energy transfer.[26–28] Spectroscopic techniques such as time-resolved spectroscopy and integrating-sphere quantum-yield measurements can provide insight into the energy transfer mechanism. Yet, these techniques are complex and not always conclusive.[29] Analysis of luminescence decay curves is a powerful method to establish the energy transfer mechanism, but requires a systematic series of high-quality samples and a quantitative model for the energy-transfer dynamics.[5,30] Integrating-sphere measurements require quantitative calibrations over a broad spectral range where the spectral response of the detector and reflective coating can vary drastically, making them prone to systematic experimental errors.[6] Moreover, this method is not ideal for screening QC phosphors in the development stage, where nonradiative losses may reduce the photon output to quantum yields below 100% despite the occurrence of QC.

In this work we use a calibration-free and universal approach to prove QC by cooperative energy transfer using single-photon time-correlated spectroscopy.[31] The creation of two excited states from a single excitation event in QC materials results in an increased likelihood of detecting pairs of photons—so-called photon bunching—on a time scale of the lifetime of the emitting state. The observation of photon bunching thus provides evidence of quantum cutting. Additionally, information about the quantum-cutting efficiency is contained within the bunching signal. Realizing these experiments in the infrared spectral range—relevant for solar-cell applications—comes with challenges due to the limited detector efficiencies, which make the likelihood of artifacts comparable to the successful detection of a QC photon pair. As a case study, we apply this method to two materials that both are claimed to be QC materials. We show that YPO_4:Tb^{3+},Yb^{3+} is indeed a QC material, whereas yttrium aluminum garnet (YAG):Ce^{3+},Yb^{3+} is not. These results are in line with the earlier modeling of time-resolved experiments by our group and showcase that our method can settle ongoing debates about quantum cutting.[19,30,32]

We study two potential QC materials, microcrystalline YPO_4 codoped with 2% Tb^{3+} and 15% Yb^{3+} and microcrystalline YAG doped with 0.1% Ce^{3+} and 5% Yb^{3+} (nominal doping concentrations). Both are claimed to perform QC by cooperative energy transfer.[5,33,34] Upon blue excitation of the sensitizer ions—Tb^{3+} or Ce^{3+}—both samples show sensitizer emission in the visible, as evident from the narrow-band emission of Tb^{3+} ($^5D_4 \rightarrow {}^7F_J$ with J = 0–5) and broadband emission of Ce^{3+} ($5d^1 \rightarrow {}^2F_{7/2}$ and $^2F_{5/2}$). Additionally, both

https://doi.org/10.1021/acsenergylett.5c01496
ACS Energy Lett. 2025, 10, 4620–4626

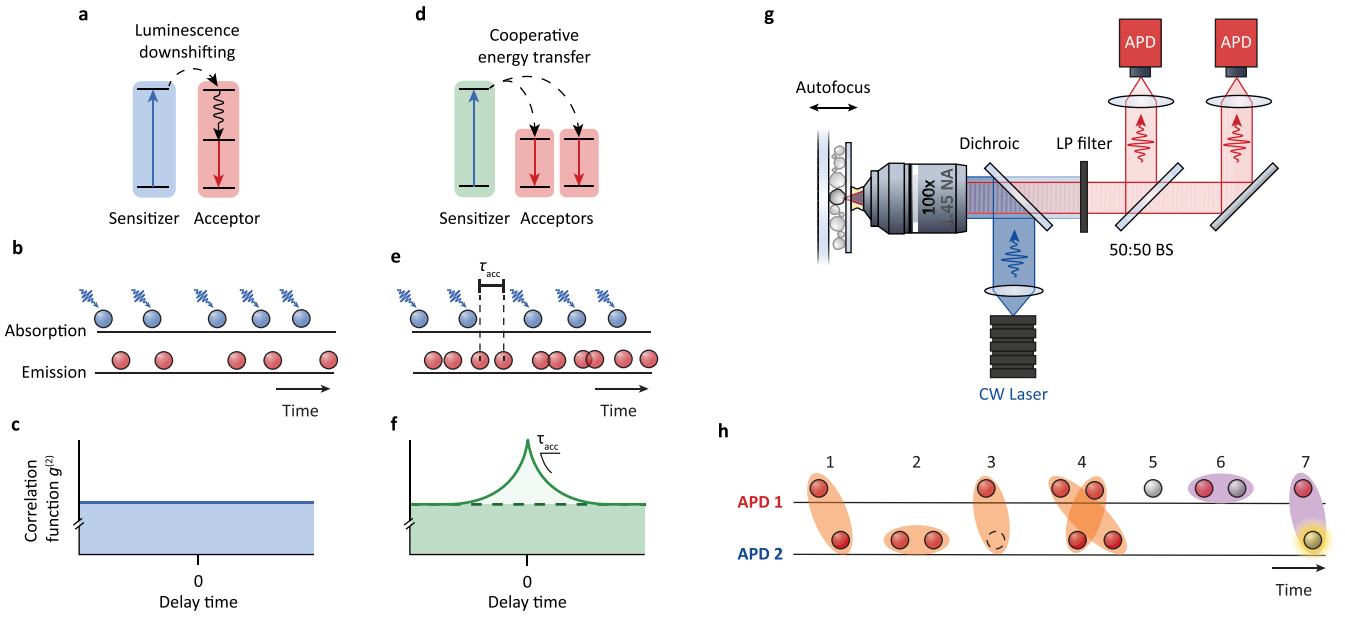

Figure 2. (a) Schematic energy level diagram for luminescence downshifting. (b) Possible photon stream shows photon emission (red) after an excitation event (blue). (c) The correlation function shows a flat curve that arises from uncorrelated photon pairs. (d–f) Same as (a)–(c), but for cooperative energy transfer. The QC material emits a photon pair for every excitation (panel e). The characteristic time difference between these photons is equal to the acceptor excited-state lifetime. The correlation function of the QC material (panel f) shows—in addition to the flat uncorrelated signal—a bunching peak due to photon pairs stemming from the same excitation event. (g) Schematic representation of the experimental setup. The sample is excited by a blue continuous-wave laser. The sample is kept in focus using a piezo stage. The collected emission light is focused onto two APDs in a Hanbury-Brown–Twiss setup. (h) Possible experimental photon stream highlighting normal operation (1–4) and undesired detector artifacts (5–7): 1. The two photons from a QC pair (orange) are detected on different detectors, contributing to the bunching signal; 2. Both photons of a QC pair are detected on the same detector; 3. Only a single photon from a QC pair is detected; 4. Photons from different pairs overlap in time; 5. Detector dark count; 6. Afterpulsing: a real detection event triggers a fake detection event on the same detector; 7. Afterglow: a real detection event results in the detector emitting a photon, which then triggers a fake detection event on the other detector. Processes 2–5 decrease the correlation in the signal, and processes 6 and 7 introduce undesired correlations (purple).

materials emit in the near-infrared at around 1000 nm (Figure 1a–d). Emission in this wavelength range can be ascribed to the Yb^{3+} $^2F_{5/2} \rightarrow {}^2F_{7/2}$ transition. We determine the excited-state lifetime τ of this transition by fitting a monoexponential function to the luminescence decay curve, using resonant excitation at 980 nm. We find $\tau = 0.6$ ms in YPO_4 and $\tau = 0.9$ ms in YAG (Figure 1e,f). The Yb^{3+} excited-state lifetime for both host materials is reported to be $\tau_r = 0.9$ ms for low-doped samples.[30,35,36] These values provide a good estimate for the radiative decay rate $k_r = 1/\tau_r$ of Yb^{3+} in these materials. Indeed, nonradiative decay due to multiphonon relaxation is expected to be inefficient as this is a 8–10th-order process in these host materials, while the low doping concentrations prevent concentration quenching by energy migration to defects.[37,38] We thus estimate a Yb^{3+} emission efficiency of $\eta_{em} = k_r\tau = 66\%$ for our YPO_4 sample and $\eta_{em} = 100\%$ for our YAG sample. While integrating-sphere measurements would be the preferred method to determine η_{em} directly, their implementation for our system is impractical. The weak absorption inherent to lanthanides, combined with the requirement for resonant excitation, makes such measurements particularly challenging.[39]

Yb^{3+} has no energy levels in the visible, so the observation of Yb^{3+} emission under blue excitation must arise from energy transfer from the sensitizer to Yb^{3+}. Sensitization is further evidenced by the observation that excitation spectra detected at the sensitizer and the activator emission show a similar line shape. Cooperative energy transfer would be energetically possible for both materials, as the sensitizer excited state lies at 2 times the Yb^{3+} excitation energy (Figure 1g,h). Indeed, this was central to previous claims of QC by cooperative energy transfer in both materials. However, based on the spectra alone we cannot be certain of the energy-transfer mechanism nor the occurrence of QC. We can only infer that energy transfer takes place.

In this work, we will use photon statistics to prove if QC by cooperative energy transfer occurs. For a non-quantum-cutting energy-transfer mechanism, a single absorption event results in at most a single emission event (Figure 2a). Under continuous-wave (CW) illumination of the sample, the optical centers absorb independently. Similarly, subsequent emission events are uncorrelated. The photon stream for such a material has an average count rate k_c and the number of emitted photons in a time interval Δt follows a Poisson distribution (Figure 2b). The corresponding second-order correlation function ($g^{(2)}$) is flat (Figure 2c), reflecting that the probability of detecting a photon, relative to a previous detection event, is constant across all time scales. In contrast, for a material capable of QC, two emission events follow from a single excitation event (Figure 2d). These photons are emitted in short succession, resulting in an increased likelihood of detecting another photon some time before or after a photon detection event (Figure 2e). In the associated $g^{(2)}$ these correlated photons will show up as a peak on top of the Poissonian background (Figure 2f). This super-Poissonian contribution is centered around a delay time of zero and falls off exponentially with a

https://doi.org/10.1021/acsenergylett.5c01496
ACS Energy Lett. 2025, 10, 4620–4626

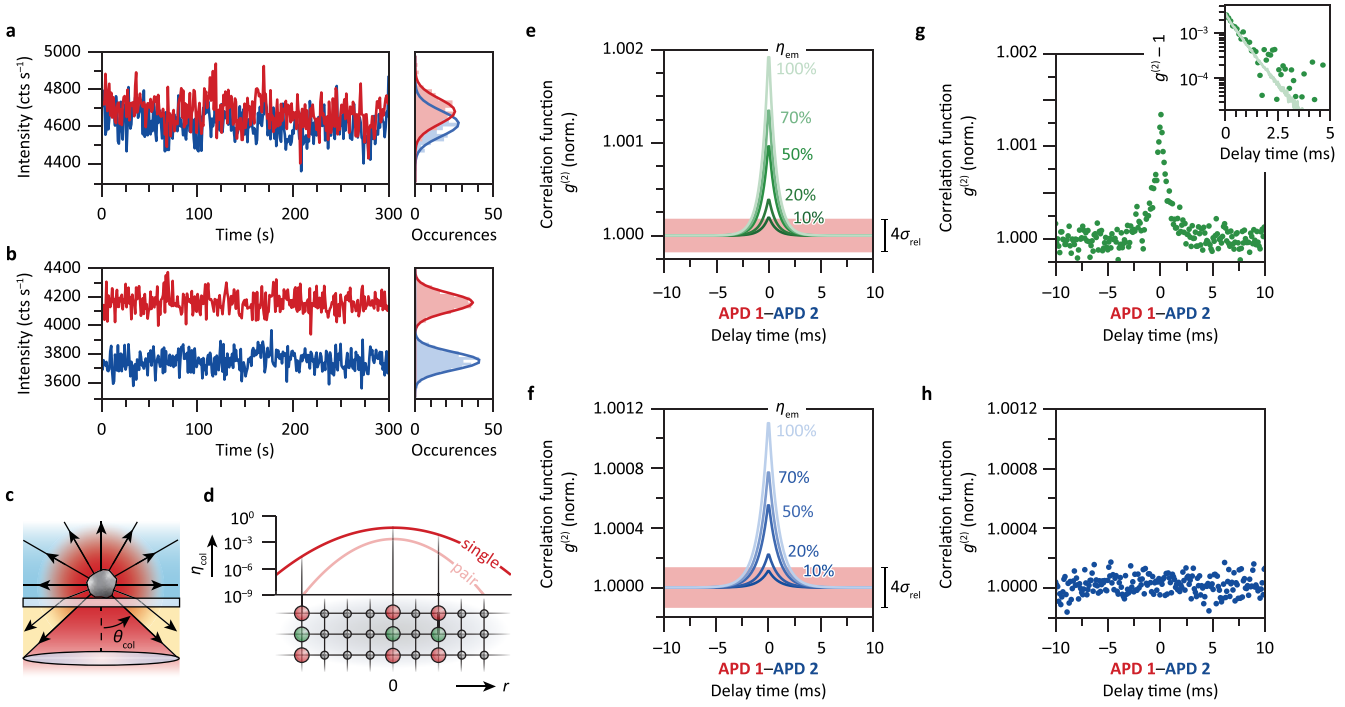

Figure 3. (a, b) Intensity traces of the signal detected on APD 1 (red) and APD 2 (blue) for the first 5 min of the measurements on (a) YAG:Ce^{3+},Yb^{3+} and (b) YPO_4:Tb^{3+},Yb^{3+}. The detector count rate distributions (right) follow statistics indistinguishable from Poissonian (solid lines). The difference in average count rate in (b) is caused by slight misalignment between detectors. (c) Cartoon illustrating the collection losses for an isotropic emission profile (black arrows). Light emitted toward the bottom half space is detected only if it falls within the detection cone with opening angle θ_{col}. (d) Cartoon illustrating collection losses stemming from a nonuniform collection profile. The curves show on a logarithmic scale the single-photon collection efficiency (red) and pair collection efficiency (light red). The single-photon detection efficiency decreases with distance from the detection focus. Therefore, the likelihood of detecting both photons from a QC center (red green circles) falls off with the square of the single-detection efficiency. (e) Expected normalized second-order correlation function for the scenario that YPO_4:Tb^{3+},Yb^{3+} exhibits QC, calculated using the experimental count rates (panel a) and the PL lifetime (Figure 1e), and considering different possible emission efficiencies η_{em} between 10 and 100%. The expected $\pm 2\sigma_{rel}$ level of the background is indicated with a red band. (f) Same as (e), but for YAG:Ce^{3+},Yb^{3+}, based on experimental count rates from panel (b) and the PL lifetime from Figure 1f. (g) Experimental normalized second-order correlation function for YPO_4:Tb^{3+},Yb^{3+}. The bunching signal is consistent with an η_{em} of 70%. The inset shows the $g^{(2)} - 1$ overlaid with the decay curve from Figure 1c. (h) Same as (g) but for YAG:Ce^{3+},Yb^{3+}. There is no discernible bunching signal above the background noise.

characteristic time scale equal to the excited state lifetime of the acceptor. See Supporting Information, Section S8 for the analytical derivation.[31]

We characterize the photon correlations using the setup shown in Figure 2g. The microcrystalline samples are excited with a blue CW laser (λ_{ex} = 488 nm for YPO_4:Tb^{3+},Yb^{3+} and λ_{ex} = 445 nm for YAG:Ce^{3+},Yb^{3+}). The excitation light is focused on the sample using an oil-immersion objective, and the resulting emission is collected by the same objective. Reflected excitation light and visible sensitizer emission are rejected using a dichroic mirror and a long-pass filter. The photon arrival times are recorded by two avalanche photodiodes (APDs) in a Hanbury-Brown–Twiss setup. The $g^{(2)}$ is constructed from the cross-correlation between the photon streams of both detectors. Shot noise limits the visibility of the bunching signal. The amplitude of the bunching signal scales with the number of correlated photon pairs in the collected emission, so ideally, the (pair) collection efficiency is maximized. Our procedure of cross-correlating the photon stream on separate detectors limits the pair detection efficiency to a theoretical maximum of 50%. Yet, two independent detectors are necessary to avoid afterpulsing artifacts, even on the Yb^{3+} excited state time scales of milliseconds (Supporting Information, Section S7). In practice, our pair detection efficiency is substantially lower than 50%. We estimate that the detection efficiency per APD is η_{col} = 2.5%. This creates a probability of $2\eta_{col}^2$ = 0.13% to detect both photons of a pair, and a much higher probability of $4\eta_{col}(1 - 2\eta_{col})$ = 9.5% to detect exactly one photon of a pair. See Supporting Information, Section S4 for the derivation. The relatively low pair detection efficiency makes long measurement times necessary to observe bunching significantly higher than noise in the Poissonian background. Detector artifacts also influence the $g^{(2)}$ (Figure 2h). Detector dark counts are a source of an uncorrelated background signal. We minimize their impact by ensuring that the count rate of real photons is at least 2 orders of magnitude higher than the dark count rate. Fake correlations in the photon stream are introduced by (1) afterpulsing, a false detection event following a real photon-detection event; and (2) afterglow, the emission of a photon by the detector. Because of the low pair collection efficiency, these artifacts can be of comparable intensity to bunching signals from quantum-cutting material. If they are not properly handled, they may be mistakenly interpreted as signatures of quantum cutting in the phosphor. The Supporting Information, Section S7 and Figure S5 explain how we correct for correlations from detector artifacts. Discerning these correlations from the QC signal requires two independent detectors.

https://doi.org/10.1021/acsenergylett.5c01496
ACS Energy Lett. 2025, 10, 4620–4626

Figure 3a,b shows intensity traces of the 980 nm Yb^{3+} emission of both materials over the course of 5 min from a 60 h measurement. The fluctuations in the count rate are indiscernible from Poisson noise. Some count-rate variations on longer time scales of hours are caused by lateral drift and limitations of our autofocus algorithm (Supporting Information, Section S5).

Based on these traces, we are able to calculate the expected correlation function for the scenario where the materials are quantum cutters. That means we can predict the magnitude of the noise on the correlation function and the amplitude of the bunching peak. Bunching is expected even for a material with a large number of dopants N and is, in fact, independent of N. Details of the calculations are given in Supporting Information, Section S8. The expected noise relative to the uncorrelated background is

$$\sigma_{\mathrm{rel}} = \frac{1}{\sqrt{\langle I_1\rangle\langle I_2\rangle T\delta t}} \tag{1}$$

Here $\langle I_1\rangle$ and $\langle I_2\rangle$ are the average count rates on detectors 1 and 2, T = 60 h is the total measurement time and δt = 100 μs is the bin width of the correlation function. The expected amplitude of the bunching peak depends on the emission efficiency η_{em} and the total excited state decay rate $k_{\mathrm{dec}} = 1/\tau$ of Yb^{3+}:

$$A_{\mathrm{rel}} = \frac{\eta_{\mathrm{em}} k_{\mathrm{dec}} \eta_{\mathrm{col},i}^{\mathrm{eff}}}{2\langle I_i\rangle} \tag{2}$$

Here $\eta_{\mathrm{col},i}^{\mathrm{eff}}$ is the effective collection efficiency of detector i for Yb^{3+} emission. This efficiency depends on the nearly isotropic emission of Yb^{3+}, which is only partially collected by the objective (Figure 3c), as well as the spatially nonuniform profiles of excitation and collection efficiency (Figure 3d). Taking these factors into consideration we estimate that $\eta_{\mathrm{col},i}^{\mathrm{eff}}$ = 0.6%, 4× smaller than the efficiency stated earlier, which was based on the collection efficiency of reflected 980 nm laser light. (see Supporting Information, Section S4). Supporting Information, Section S8 gives more detail about the calculation of $\eta_{\mathrm{col},i}^{\mathrm{eff}}$. To exclude quenching of Yb^{3+} via saturation-induced quenching pathways we choose an excitation power far below the saturation threshold (see Supporting Information, Section S6).

Figure 3e,f shows the expected normalized correlation function of YPO_4:Tb^{3+},Yb^{3+} and YAG:Ce^{3+},Yb^{3+} calculated considering different possible values for the emission efficiency η_{em}. The expected relative noise (eq 1) is represented by the bandwidth $\pm 2\sigma_{\mathrm{rel}}$ centered on the uncorrelated background level. The bunching peak amplitude (eq 2) depends on η_{em} and the curve decreases exponentially with the total decay rate k_{dec}, as determined earlier (Figure 1). Figure 3e,f shows that the photon bunching peak should be visible above the noise if (1) the sample exhibits QC and (2) the η_{em} of Yb^{3+} exceeds 10%.

Figure 3g,h shows the experimental correlation functions for YPO_4:Tb^{3+},Yb^{3+} (Figure 3g) and YAG:Ce^{3+},Yb^{3+} (Figure 3h). The correlation function of YPO_4:Tb^{3+},Yb^{3+} closely matches the theoretical bunching signal for an emission efficiency of η_{em} = 70%, which aligns well with the 66% efficiency determined from the lifetime measurement. Although the lifetime analysis (Figure 1e) depended on assumptions, the close agreement with the efficiency extracted from the correlation analysis (Figure 3e,g) provides additional confidence in the correlation measurements. These results confirm that YPO_4:Tb^{3+},Yb^{3+} is a QC phosphor.

In contrast, the experimental correlation function of YAG:Ce^{3+},Yb^{3+} shows no significant bunching signal. While the expected bunching signal due to QC would be obscured by noise if the Yb^{3+} emission efficiency were η_{em} = 10% or lower (Figure 3f), the Yb^{3+} lifetime of 0.9 ms (Figure 1h) shows that η_{em} is close to 100%. Hence, QC by Yb^{3+} sensitization through a cooperative energy-transfer mechanism would produce an expected bunching amplitude of 20× the background noise. The absence of such bunching in our experiment on YAG:Ce^{3+},Yb^{3+} is clear evidence against previous claims that the material is a QC phosphor through cooperative energy transfer.[33,34] These result support earlier conclusion by Yu et al. and Ueda et al., who raised doubts against claims of QC by YAG:Ce^{3+},Yb^{3+}.[30,32]

Our analysis of eqs 1 and 2, illustrated in Figure 3e,f, shows that the noise level in our experiments is sufficiently low to correctly prove or disprove quantum cutting in our materials. This is critical to our conclusions about the energy-transfer processes in YPO_4:Tb^{3+},Yb^{3+} and YAG:Ce^{3+},Yb^{3+}. More generally, eqs 1 and 2 can be used to assess whether a measurement is sufficiently sensitive to detect quantum cutting with statistical significance. If the noise (eq 1) exceeds the expected bunching amplitude (eq 2), one could change the experiment in two ways. (1) Increasing the measurement time T reduces the relative noise. This is conceptually simple, but the noise decreases slowly as $1/\sqrt{T}$. (2) Alternatively, improving the optical setup could boost η_{col}. This has a stronger positive effect; however, it may be practically more challenging. This could, for example, require detectors with increased spectral response at the emission wavelength or fewer and more efficient optical elements in the detection arm of the setup.

In summary, we have demonstrated how photon statistics can be used as a universal test to determine if a near-infrared-emitting material performs QC. As a case study, we applied our technique to two purported QC materials, YAG:Ce^{3+},Yb^{3+} and YPO_4:Tb^{3+},Yb^{3+}. The photon statistics of the Yb^{3+} emission are qualitatively different between the two materials, showing that one material is an efficient QC phosphor while the other is not. Specifically, YPO_4:Tb^{3+},Yb^{3+} shows photon bunching, consistent with QC by cooperative energy transfer. The photon bunching amplitude has the expected magnitude, calculated based on calibration of our experimental setup. In contrast, YAG:Ce^{3+},Yb^{3+} shows no photon bunching, while a bunching amplitude 20× higher than the background noise was expected. We conclude that, in contradiction with previous claims but in line with the findings of Yu et al. and Ueda et al., YAG:Ce^{3+},Yb^{3+} is not a QC phosphor.[30,32−34] This work provides the community with a universal and systematic approach to efficiently identify NIR-emitting phosphors suitable for use in quantum-cutting layers for photovoltaic applications. This method would lend itself for quantifying the QC capabilities of singlet-fission dyes, nonresonantly excited quantum dots, Yb-containing organic complexes, or Yb-doped perovskites.

https://doi.org/10.1021/acsenergylett.5c01496
ACS Energy Lett. 2025, 10, 4620−4626

■ ASSOCIATED CONTENT

Data Availability Statement

The source data that supports the findings in this work can be downloaded from the Zenodo server (DOI: 10.5281/zenodo.16991188).

Supporting Information

The Supporting Information is available free of charge at https://pubs.acs.org/doi/10.1021/acsenergylett.5c01496.

Sample fabrication and characterization, experimental methods, collection efficiency calculations, saturation measurements, discussion of detector artifacts and correction procedure, derivation of analytical expression for $g^{(2)}$ (PDF)

■ AUTHOR INFORMATION

Corresponding Author

Freddy T. Rabouw − *Soft Condensed Matter and Biophysics, Debye Institute for Nanomaterials Science and Condensed Matter and Interfaces, Debye Institute for Nanomaterials Science, Utrecht University, 3584 CC, Utrecht, The Netherlands;* orcid.org/0000-0002-4775-0859; Email: f.t.rabouw@uu.nl

Authors

Vincent R.M. Benning − *Soft Condensed Matter and Biophysics, Debye Institute for Nanomaterials Science and Condensed Matter and Interfaces, Debye Institute for Nanomaterials Science, Utrecht University, 3584 CC, Utrecht, The Netherlands*

Nils van de Mortel − *Soft Condensed Matter and Biophysics, Debye Institute for Nanomaterials Science, Utrecht University, 3584 CC, Utrecht, The Netherlands*

Midas Waakop Reijers − *Soft Condensed Matter and Biophysics, Debye Institute for Nanomaterials Science, Utrecht University, 3584 CC, Utrecht, The Netherlands*

Maurits Mastwijk − *Condensed Matter and Interfaces, Debye Institute for Nanomaterials Science, Utrecht University, 3584 CC, Utrecht, The Netherlands*

Sander J.W. Vonk − *Optical Materials Engineering Laboratory, Department of Mechanical and Process Engineering, ETH Zurich, 8092 Zurich, Switzerland;* orcid.org/0000-0002-4650-9473

Andries Meijerink − *Condensed Matter and Interfaces, Debye Institute for Nanomaterials Science, Utrecht University, 3584 CC, Utrecht, The Netherlands;* orcid.org/0000-0003-3573-9289

Complete contact information is available at: https://pubs.acs.org/10.1021/acsenergylett.5c01496

Notes

The authors declare no competing financial interest.

■ ACKNOWLEDGMENTS

This work was supported by NWO Grant Vi.Vidi.203.031 (VRMB, main applicant FTR).

■ REFERENCES

(1) Setlur, A. A. Phosphors for LED-based solid-state lighting. *Electrochem. Soc. Interface.* **2009**, *18*, 32.

(2) Wang, L.; et al. Highly efficient narrow-band green and red phosphors enabling wider color-gamut LED backlight for more brilliant displays. *Opt. Express.* **2015**, *23*, 28707−28717.

(3) Serrano, D.; et al. Ytterbium sensitization in KY_3F_{10}: Pr^{3+}, Yb^{3+} for silicon solar cells efficiency enhancement. *Opt. Mater.* **2011**, *33*, 1028−1031.

(4) Milstein, T. J.; Kroupa, D. M.; Gamelin, D. R. Picosecond quantum cutting generates photoluminescence quantum yields over 100% in ytterbium-doped $CsPbCl_3$ nanocrystals. *Nano Lett.* **2018**, *18*, 3792−3799.

(5) Vergeer, P.; et al. Quantum cutting by cooperative energy transfer in $Yb_x Y_{1-x} PO_4$: Tb^{3+}. *Phys. Rev. B Condens. Matter* **2005**, *71*, 014119.

(6) Zhydachevskyy, Y.; et al. Quantum efficiency of the down-conversion process in Bi^{3+}−Yb^{3+} and Ce^{3+}−Yb^{3+} co-doped garnets. *Sol. Energy Mater. Sol. Cells* **2018**, *185*, 240−251.

(7) Sanders, S. N.; et al. Intramolecular singlet fission in oligoacene heterodimers. *Angew. Chem.* **2016**, *128*, 3434−3438.

(8) Schaller, R. D.; Sykora, M.; Jeong, S.; Klimov, V. I. High-efficiency carrier multiplication and ultrafast charge separation in semiconductor nanocrystals studied via time-resolved photoluminescence. *J. Phys. Chem. B* **2006**, *110*, 25332−25338.

(9) Schaller, R. D.; Pietryga, J. M.; Klimov, V. I. Carrier multiplication in InAs nanocrystal quantum dots with an onset defined by the energy conservation limit. *Nano Lett.* **2007**, *7*, 3469−3476.

(10) Samhadaneh, D. M.; et al. Evaluation of lanthanide-doped upconverting nanoparticles for in vitro and in vivo applications. *ACS Appl. Bio. Mater.* **2020**, *3*, 4358−4369.

(11) Jin, S.; et al. A new near infrared photosensitizing nanoplatform containing blue-emitting up-conversion nanoparticles and hypocrellin A for photodynamic therapy of cancer cells. *Nanoscale* **2013**, *5*, 11910−11918.

(12) Kim, Y. H.; et al. A zero-thermal-quenching phosphor. *Nat. Mater.* **2017**, *16*, 543−550.

(13) Berends, A. C.; van de Haar, M. A.; Krames, M. R. YAG: Ce^{3+} phosphor: from micron-sized workhorse for general lighting to a bright future on the nanoscale. *Chem. Rev.* **2020**, *120*, 13461−13479.

(14) Li, M.; Begum, R.; Fu, J.; Xu, Q.; Koh, T. M.; Veldhuis, S. A.; Gratzel, M.; Mathews, N.; Mhaisalkar, S.; Sum, T. C. Low threshold and efficient multiple exciton generation in halide perovskite nanocrystals. *Nat. Commun.* **2018**, *9*, 4197.

(15) Pazos-Outón, L. M.; et al. A silicon−singlet fission tandem solar cell exceeding 100% external quantum efficiency with high spectral stability. *ACS Energy Lett.* **2017**, *2*, 476−480.

(16) Wegh, R. T.; Donker, H.; Oskam, K. D.; Meijerink, A. Visible quantum cutting in $LiGdF_4$: Eu^{3+} through downconversion. *Science* **1999**, *283*, 663−666.

(17) Liu, B.; Chen, Y.; Shi, C.; Tang, H.; Tao, Y. Visible quantum cutting in BaF_2: Gd, Eu via downconversion. *J. Lumin.* **2003**, *101*, 155−159.

(18) Oskam, K.; Wegh, R.; Donker, H.; Van Loef, E.; Meijerink, A. Downconversion: a new route to visible quantum cutting. *J. Alloys Compd.* **2000**, *300*, 421−425.

(19) Wegh, R. T.; Donker, H.; Meijerink, A.; Lamminmäki, R. J.; Hölsä, J. Vacuum-ultraviolet spectroscopy and quantum cutting for Gd^{3+} in $LiYF_4$. *Phys. Rev. B* **1997**, *56*, 13841−13848.

(20) Shockley, W.; Queisser, H. J. Detailed balance limit of efficiency of p−n junction solar cells. *J. Appl. Phys.* **1961**, *32*, 510.

(21) Wu, D.; Dong, X.; Xiao, W.; Hao, Z.; Zhang, J. Efficient visible-to-NIR spectral conversion for polycrystalline Si solar cells and revisiting the energy transfer mechanism from Ce^{3+} to Yb^{3+} in $Lu_3Al_5O_{12}$ host. *Inorg. Chem.* **2019**, *58*, 234−242.

(22) Jiménez, J. A. Monovalent copper-mediated UV to NIR luminescence down-shifting in Yb^{3+}-doped glass. *J. Mater. Chem. C* **2022**, *10*, 15466−15473.

(23) Zhou, J.; Teng, Y.; Ye, S.; Liu, X.; Qiu, J. Broadband down-conversion spectral modification based on energy transfer. *Opt. Mater.* **2010**, *33*, 153−158.

(24) de Wit, J. W.; Sonneveld, L. L.; Meijerink, A. Shedding light on host-to-Yb^{3+} energy transfer in $Cs_2AgBiBr_6$: Yb^{3+} (nano) crystals. *Chem. Mater.* **2024**, *36*, 2857−2866.

(25) Klik, M. A. J.; Gregorkiewicz, T.; Bradley, I. V.; Wells, J.-P. R. Optically induced deexcitation of rare-earth ions in a semiconductor matrix. *Phys. Rev. Lett.* **2002**, *89*, 227401.
(26) Singh, P.; Modanwal, S.; Mishra, H.; Rai, S. Upconversion, downshifting, quantum cutting and back energy transfer from Yb^{3+} to Er^{3+} in Er^{3+}/Yb^{3+} co-doped $CaTiO_3$ phosphor, intense NIR generation for communication. *Ceram. Int.* **2024**, *50*, 32206−32216.
(27) Chen, J.; Guo, H.; Li, Z.; Zhang, H.; Zhuang, Y. Near-infrared quantum cutting in Ce^{3+}, Yb^{3+} co-doped YBO_3 phosphors by cooperative energy transfer. *Opt. Mater.* **2010**, *32*, 998−1001.
(28) Chen, X.; Huang, X.; Zhang, Q. Concentration-dependent near-infrared quantum cutting in $NaYF_4$: Pr^{3+}, Yb^{3+} phosphor. *J. Appl. Phys.* **2009**, *106*, 063518.
(29) Tyagi, P.; Kambhampati, P. False multiple exciton recombination and multiple exciton generation signals in semiconductor quantum dots arise from surface charge trapping. *J. Chem. Phys.* **2011**, *134*, 094706.
(30) Yu, D.; et al. Insights into the energy transfer mechanism in Ce^{3+}-Yb^{3+} codoped YAG phosphors. *Phys. Rev. B* **2014**, *90*, 165126.
(31) De Jong, M.; Meijerink, A.; Rabouw, F. T. Non-poissonian photon statistics from macroscopic photon cutting materials. *Nat. Commun.* **2017**, *8*, 15537.
(32) Ueda, J.; Tanabe, S. Visible to near infrared conversion in Ce^{3+}−Yb^{3+} co-doped YAG ceramics. *J. Appl. Phys.* **2009**, *106*, 043101.
(33) Tai, Y.; Li, X.; Du, X.; Pan, B.; Yuan, G. Broadband near-infrared quantum cutting by Ce−Yb codoped YAG transparent glass ceramics for silicon solar cells. *RSC Adv.* **2018**, *8*, 23268−23273.
(34) Lin, H.; Zhou, S.; Teng, H.; Li, Y.; Li, W.; Hou, X.; Jia, T. Near infrared quantum cutting in heavy Yb doped $Ce_{0.03}Yb_{3x}Y_{(2.97-3x)}Al_5O_{12}$ transparent ceramics for crystalline silicon solar cells. *J. Appl. Phys.* **2010**, *107*, 043107.
(35) Ubizskii, S.; et al. Optical properties of epitaxial YAG: Yb films. *Phys. Status Solidi A Appl. Res.* **2004**, *201*, 791−797.
(36) Kaminska, A.; Duzynska, A.; Suchocki, A.; Bettinelli, M. Spectroscopy of f−f radiative transitions of Yb^{3+} ions in ytterbium doped orthophosphates at ambient and high hydrostatic pressures. *J. Phys.: Condens. Matter* **2010**, *22*, 225902.
(37) Auzel, F.; Baldacchini, G.; Laversenne, L.; Boulon, G. Radiation trapping and self-quenching analysis in Yb^{3+}, Er^{3+}, and Ho^{3+} doped Y_2O_3. *Opt. Mater.* **2003**, *24*, 103−109.
(38) Van Dijk, J.; Schuurmans, M. On the nonradiative and radiative decay rates and a modified exponential energy gap law for 4 f−4 f transitions in rare-earth ions. *J. Chem. Phys.* **1983**, *78*, 5317−5323.
(39) van Dam, B.; et al. Quantum yield bias in materials with lower absorptance. *Phys. Rev. Appl.* **2019**, *12*, 024022.

https://doi.org/10.1021/acsenergylett.5c01496
ACS Energy Lett. 2025, 10, 4620−4626